NANO LETTERS

Communication

Hofstadter Butterfly and Many body effects in epitaxial graphene superlattice

Wei Yang, Xiaobo Lu, Guorui Chen, Shuang Wu, Guibai Xie, Meng Cheng, Duoming Wang, Rong Yang, Dongxia Shi, Kenji Watanabe, Takashi Taniguchi, Christophe Voisin, Bernard Placais, Yuanbo Zhang, and Guangyu Zhang

Nano Lett., **Just Accepted Manuscript** • DOI: 10.1021/acs.nanolett.5b05161 • Publication Date (Web): 07 Mar 2016

ACS Publications

Nano Letters is published by the American Chemical Society. 1155 Sixteenth Street N.W., Washington, DC 20036

Hofstadter Butterfly and Many body effects in epitaxial graphene superlattice

Wei Yang[1,2], Xiaobo Lu[1], Guorui Chen[3], Shuang Wu[1], Guibai Xie[1], Meng Cheng[1], Duoming Wang[1], Rong Yang[1], Dongxia Shi[1], Kenji Watanabe[4], Takashi Taniguchi[4], Christophe Voisin[2], Bernard Plaçais[2], Yuanbo Zhang[3], and Guangyu Zhang[1]*

[1] *Beijing National Laboratory for Condensed Matter Physics and Institute of Physics, Chinese Academy of Sciences, Beijing 100190, China.*
[2] *Laboratoire Pierre Aigrain, Ecole Normale Supérieure-PSL Research University, CNRS, Université Pierre et Marie Curie-Sorbonne Universités, Université Paris Diderot-Sorbonne Paris Cité, 24 rue Lhomond, 75231 Paris Cedex 05, France.*
[3] *State Key Laboratory of Surface Physics and Department of Physics, Fudan University, Shanghai 200433, China.*
[4] *Advanced Materials Laboratory, National Institute for Materials Science, 1-1 Namiki, Tsukuba, 305-0044, Japan.*

Abstract: Graphene placed on h-BN has received a wide range of interests due to the improved electrical performance and rich physics from the interface, especially the emergence of superlattice Dirac points as well as Hofstadter butterfly in high magnetic field. Instead of transferring graphene onto h-BN, epitaxial growth of graphene directly on a single-crystal h-BN provides an alternative and promising way to study these interesting superlattice effects due to their precise lattice alignment. Here we report an electrical transport study on epitaxial graphene superlattice on h-BN with a period of ~15.6 nm. The epitaxial graphene superlattice is clean, intrinsic, and of high quality with a carrier mobility of ~27,000 $cm^2V^{-1}s^{-1}$, enabling to observe Hofstadter butterfly features originated from the superlattice at a magnetic field as low as 6.4 T. A metal-insulator transition and magnetic field dependent Fermi velocity were also observed, suggesting prominent electron-electron interaction-induced many body effects.

Key words: Graphene superlattice, Hofstadter butterfly, Metal-insulator transition, Fermi velocity, Many body effect

Due to the 2D nature of graphene[1, 2], interfaces play an important role in modulation of graphene's electronic properties. By placing graphene on top of hexagonal boron nitride (h-BN), a rather clean and flat interface could be achieved, leading to a suppressed charge inhomogeneity and an enhanced mobility[3, 4]. Such clean interfaces would introduce strong electron-electron (e-e) interaction, causing metal insulator transition (MIT)[5, 6], quantum Hall ferromagnetism (QHFM)[7-9] and Fermi velocity renormalization in graphene[10-12]. When the relative lattice rotation angle between graphene and h-BN approaches zero, the lattice mismatch induced moiré pattern has the largest period, i.e. λ~15nm[13]. This moiré pattern is more than a geometrical superstructure, and it brings a periodic potential modulation to the original graphene lattice and reshapes the band structure of graphene by producing superlattice minibands[13-19]. The quantum Hall effect (QHE) in such moiré superlattice has a phase diagram with a fractal structure, so called Hofstadter butterfly[17-24]. It has been experimentally observed that the magnetic minibands repeat in a self-similar way at rational values $\Phi/\Phi_0=p/q$, where Φ is the magnetic flux through the superlattice unit cell, $\Phi_0=h/e$ is the magnetic flux quantum, and p, q are integers[17-19]. The description of the fractal spectra involves the introduction of Diophantine relation $n/n_0 = t(\Phi/\Phi_0)+s$, where t and s are integers referred to superlattice minibands index[17, 18], with $n_0=1/A$, $A=\sqrt{3}\lambda^2/2$ the area of superlattice unit cell, and n the carrier density. Usually, the experimental access to Hofstadter butterfly spectrum is difficult, thus a clean interface between graphene and h-BN with a nearly zero lattice rotation angle is highly desired to study the Hofstadter butterfly features at low magnetic fields.

In this paper, we present the magneto-transport measurements of the precisely aligned graphene on h-BN (G/h-BN). The zero-twisted G/h-BN samples with clean and intrinsic interfaces were prepared by Van der Waals epitaxial growth technique[13]. We identified typically two kinds of Hofstadter butterfly gaps aside from the single particle gap[25, 26] and the many body QFHM gap[7, 8] with Landau levels (LLs) from the main Dirac point (DP). The first ones are fanned out from the superlattice Dirac points (SDPs), similar to LLs fanned out from the DP, and they are Hofstadter minibands in the regime of strong superlattice modulation[22]. While the second ones are the gaps generated from the intersections of LLs from DP and SDPs and are attributed to LLs originating from replica Dirac spectra quantized in the effective magnetic field, B_{eff}[17-19, 22]. Here, $B_{eff}=\pm|B-B_{1/q}|$ with q=3 and 4, which correspond to a magnetic field of 6.4 T and 4.8 T, respectively. Note that both single particle and many body gaps contribute to the observed Hofstadter minibands, suggesting strong e-e interactions in our epitaxial G/h-BN samples. More experimental evidences of e-e interactions are provided in a metal insulator transition (MIT) over a wide range of carrier density at a temperature of around 30K, as well as a magnetic field dependent Fermi velocity.

Figure 1a shows a Hall bar device fabricated from the epitaxial G/h-BN. The thickness of h-BN flake (exfoliated on 300nm SiO_2/(p++)Si substrate) is ~70 nm. Monolayer graphene was epitaxially grown on h-BN by a low temperature plasma-enhanced chemical vapor deposition (PECVD) technique[13]. The as-grown graphene is single crystalline and its lattice rotation relative to the underneath h-BN is zero. Moiré superlattice with a period of ~15.6 nm is shown in the atomic force microscopy (AFM) height image (Fig. 1b). Standard electron beam lithography, contact metal deposition (100nm-Au/2nm-Ti) and lift-off techniques were utilized for device fabrications. Note that no reactive ion etching (RIE) was applied during the device fabrication process in order to avoid any possible structural damages or external contaminations to the device. Fig. 1c shows a typical transfer curve of the device at T=1.8K. Dirac point locates at V_g=-0.4V, indicating negligible doping; and it shows a very narrow resistance peak with an estimated electron mobility of ~27,000 $cm^2V^{-1}s^{-1}$, which is about 5 times higher than that of our previously reported device in ref.13 with a RIE process. The SDPs can be seen at both electron and hole side (Fig. 1c) as two satellite resistance peaks beside the main Dirac point with ΔV_g=~36 V. Similar to the previous findings[13, 16-19], these two resistance peaks are strongly asymmetric.

Figure 2a depicts a quantum Hall fan diagram with a color mapping of R_{xx} with respect to the gate voltages and magnetic fields at a temperature of T=1.8K. LLs from Dirac fermions can be clearly identified as the resistance minima fanning out from DP, including both normal quantum Hall (QH) states (ν = 4n+2, where n=0, ±1, ±2… is LL index) and symmetry broken QH states (ν = 0, ±1, and 4n). A line cut of Fig. 2a at B=~9T is shown in Fig. 2b and a lift of LLs degeneracy is clearly demonstrated in the inset of Fig. 2b as symmetry broken states develops at ν=0, ±1, and ν = 4n at higher carrier densities. Particularly, the onset of ν=1 state starts as low as 3T (Supplementary Fig. S2). The emergence of these symmetry broken states at such a low magnetic field is due to two possible reasons: the moiré potential induced breaking of sublattice symmetry[18] and the e-e interaction induced many body QHFM gaps[7, 22, 27, 28]. Note that a breaking of sublattice symmetry would also induce an energy gap at main DP[18]; however we didn't see any obvious gap features in our transport data, indicating this factor makes little contribution. On the other hand, the e-e interactions are estimated to be more pronounced owing to the clean and intrinsic interface between graphene and hBN. Thus, we attribute the observed symmetry broken states mainly from the nontrivial e-e interaction induced QHFM gaps.

It is also worth noting that a mapping of R_{xx} alone is not sufficient to identify Hofstadter butterfly states; thus, we take Hall resistance into account and plot a color mapping of longitudinal conductance $\sigma_{xx} = R_{xx}/(R_{xx}^2+R_{xy}^2)$ and Hall conductance $\sigma_{xy}= R_{xy}/(R_{xx}^2+R_{xy}^2)$. Figure 3a and 3b are the resulted mappings of σ_{xx} and σ_{xy} respectively, with the color contrast chosen to favor superlattice related QH states. The QH states are characterized by those σ_{xx} minima and σ_{xy} plateaus.

From these mappings, we can see that there are typically two kinds of Hofstadter butterfly gaps. The first ones are LLs like gaps fanned out from the SDPs, similar to gaps fanned out from the DP, and they are called Hofstadter minibands in the regime of strong superlattice modulation[22, 23]. These gaps are indicated by the white dashed lines in left panel of Fig. 3c, e.g. gaps from the SDP with ν_s= 0, ±2 are clearly depicted as three trenches of σ_{xx} minima. The second ones are the gaps that can't be traced back to either the DP or the SDPs, and they can be described as landau levels originating from replica Dirac spectra that are quantized in effective magnetic field $B_{eff} = \pm|B-B_{1/q}|$[17-19, 22]. These Hofstadter gaps are clearly revealed at $B=B_{1/3}$=6.4T, where new gaps are generated at the intersection of LLs from the DP and that from the SDP. For example, the intersection of ν = -10 (grey dashed line) and ν_s=2 (white dashed line) is shown in Fig. 3c. However, a small deviation can be found between the fractal Hofstadter bands and the LLs from the DP at ν=-16 and the SDP at ν_s=-4, indicated by black arrow in Fig. 3c. The deviation might be caused by the influence of a higher order superlattice effect outside of the first mini-Brillouin zone, a second generation of SDP (SSDP) as indicated in Figure S7. As a result, the spectra would be more complicated since DP, SDP, and SSDP are not equally spaced (the ratio of their spacing is 1: (√3-1)).

Details of the gaps are summarized in the Wannier diagram[29] as shown in Fig. 3d, where normalized density n/n_0 is used as X- axis. The main DP is situated at $n/n_0 = 0$, from which LLs are fanned out as the black (single particle gaps) and the blue (many body gaps) lines. The SDPs are located at $n/n_0 = \pm4$, and similarly from which LLs like Hofstadter minibands in the regime of strong superlattice modulation are developed including symmetry conserved (green lines) and symmetry broken (pink lines) gaps. The fractal Hofstadter spectra that experienced in a reduced effective magnetic field $B_{eff}=\pm|B-B_{1/q}|$ are labeled as red lines with q=1/3 and q=1/4. The distribution of gaps in Fig. 3d agrees with the theory[23] in that, for $\Phi/\Phi_0<1/5$, all the gaps can be traced back to analytically LLs of DP or SDPs. The fractal Hofstadter butterfly spectra show up until $\Phi/\Phi_0>1/5$. Besides, the gaps observed in our epitaxial G/hBN samples display quite strong thermal stability; fractal gaps at $\Phi/\Phi_0=1/3$ can stay visible at T=30K (see Supplementary Figure S2) while the gaps at $v_s=\pm2$ from SDP at hole side are very stable up to T>40K.

The observation of Hofstadter butterfly spectra at such low magnetic field can be attributed to the combination of: 1) a strong superlattice modulation; 2) a strong e-e interaction[30]; and 3) a reduction of extra carrier scattering from substrate due to ultra clean interface. The strong superlattice modulation is evidenced by the LLs fanning out from SDP; while the strong e-e interaction is demonstrated in those symmetry broken states originated from both DP and SDP. In fact, the strong e-e interactions are also manifested in observation of MIT and magnetic field dependent Fermi velocity.

Figure 4a shows a mapping of $R_{xx}(T)/R_{xx}(T=1.8K)$ at various carrier densities. At around DP and SDP as well within a gate modulation range of 4V, it behaves like insulator as the resistances increase all the way up as T drops down (inset of Fig. 4b), which agrees well with the literatures[3]. However, away from these regions, the resistances first decrease and then increase after T drops down to a critical point, suggesting a metal-insulator transition (MIT)[5]. The transition temperature is usually from 10K to 30K depending on the position of Fermi level. The trend is that the closer to charge neutrality points (DP or SDP) the higher the transition temperature. Similar to the literature[6], the MIT in graphene occurs with decreasing rather than increasing the charge inhomogeneity. However, our results are different from the literature in two aspects. Firstly, there is no screening layer in our device; instead, we utilized the epitaxial G/h-BN with an intrinsic interface in this study. Secondly, the MIT observed in our device occurs over a wide range of charge carrier densities. The observations can be attributed to the onset of quantum interference[31, 32] and the superlattice modulation. The former makes electrons constrained or localized[33-35], leading to the observed transition within a wide range of carrier densities at low temperature. While the latter produces extra charge neutral points (i.e. SDPs) close to the DP as well as a density of state discontinuity in between, so called Van Hove singularities[16, 36, 37], which in turn modulate the specific conducting behaviors of electrons and contribute to the sharp and prominent MIT close to these charge neutral points.

Figure 5a plots Shubnikov–de Haas oscillations (SdHOs) versus magnetic fields at V_g=20V for temperature from 1.8 K to 80 K, where v_F is extracted from temperature dependent amplitudes[25] as shown in the inset for B=3T (corresponding to ν=14). The result is displayed as blue stars in Fig. 5b that v_F is decreased from 1.36×10^6 m/s to 0.86×10^6 m/s as magnetic field is increased from 2.3 T to 7 T. Note that we limit the gate voltage $|V_g|$=20V to minimize the influence from superlattice. Such a magnetic field dependent Fermi velocity is beyond the scope of single particle picture, and it indicates strong many body interactions[10-12]. The finding also agrees well with magneto-optical LL transitions[38, 39].

In conclusion, we studied the transport properties of graphene superlattice obtained from epitaxial growth. The clean interface between graphene and h-BN allows us to reveal a nice picture of fractal gaps of Hofstadter butterfly developed with the filling of magnetic flux in a unit superlattice cell at a magnetic field as low as 6.4 T (corresponding to a filling of 1/3 quantum flux), which has not been explored in literature[17-19, 22]. Such intrinsic interface also gives a clue of strong e-e interactions, as evidenced by the observed MIT over a wide range of carrier densities and a renormalization of Fermi velocity to the magnetic field. Therefore, our results indicate an important role of the interface in 2D atomic crystal heterostructure on their electronic properties.

Methods

Epitaxial growth of graphene on h-BN. h-BN flakes were prepared by mechanical exfoliation of h-BN crystals onto 300-nm SiO_2/Si substrate by Scotch tape. And then graphene was epitaxially grown on top of hBN in PECVD with a low temperature of ~500 ^{o}C as described in ref.13. The resulting graphene superlattice structure was characterized by AFM (MultiMode IIId, Veeco Instruments Inc.) using tapping mode under ambient condition.

Devices fabrication and electric measurements for G/h-BN. As-grown G/h-BN samples were first spin-coated with Polymethylmethacrylate (PMMA) photoresist, followed by electron beam lithography (EBL) to define electrodes. Reactive ion etching process of graphene was avoided by putting contacts at the edge of G/h-BN in

Hall bar geometry. Devices were then fabricated with contact metal (100nm-Au/2nm-Ti) deposition via electron beam evaporation and following standard metal lift-off technique. Transport and magnetotransport measurements were carried out in cryogenic Dewar (Janis) using standard lock-in technique (Stanford).

Acknowledgements

G.Z. acknowledges supports of the National Basic Research Program of China (973 Program) under the grant No. 2013CB934500 and 2012CB921302, the National Science Foundation of China (NSFC) under the grant No. 91223204. Y.Z. acknowledges supports of 973 Program of China under the grant No. 2011CB921802 and NSF of China under the grant No. 11034001.

Supporting Information

The Supporting Information provides thermal stability of QH states, onset of $\nu = 0, 1$ at a low magnetic field, conductance at $\Phi=\Phi_{1/3}$, influence of quantum capacitance, weak localization effects, Femi velocity measurements, and observation of a second generation of superlattice Dirac points.

Corresponding Author

* E-mai: (G.Z.) gyzhang@aphy.iphy.ac.cn.

Author Contributions

G.Z. and W.Y. designed the research; W.Y. performed the growth, structural characterization, device fabrication, and electrical transport measurements; X.L. helped on graphene growth; G.C provided the h-BN substrates; K.W. and T.T. synthesized h-BN crystals. W.Y., G.Z. analysed data and wrote the manuscript, and all authors discussed and commented on the paper.

Notes

The authors declare no competing financial interests.

References

1. Novoselov, K. S.; Geim, A. K.; Morozov, S. V.; Jiang, D.; Zhang, Y.; Dubonos, S. V.; Grigorieva, I. V.; Firsov, A. A. *Science* **2004,** 306, 666-669.

2. Castro Neto, A. H.; Guinea, F.; Peres, N. M. R.; Novoselov, K. S.; Geim, A. K. *Rev. of Mod. Phys.* **2009,** 81, 109-162.
3. Dean, C. R.; Young, A. F.; Meric, I.; Lee, C.; Wang, L.; Sorgenfrei, S.; Watanabe, K.; Taniguchi, T.; Kim, P.; Shepard, K. L.; Hone, J. *Nat. Nanotech.* **2010,** 5, 722-726.
4. Wang, L.; Meric, I.; Huang, P. Y.; Gao, Q.; Gao, Y.; Tran, H.; Taniguchi, T.; Watanabe, K.; Campos, L. M.; Muller, D. A.; Guo, J.; Kim, P.; Hone, J.; Shepard, K. L.; Dean, C. R. *Science* **2013,** 342, 614-617.
5. Mott, N. F. *Rev. of Mod. Phys.* **1968,** 40, 677-683.
6. Ponomarenko, L. A.; Geim, A. K.; Zhukov, A. A.; Jalil, R.; Morozov, S. V.; Novoselov, K. S.; Grigorieva, I. V.; Hill, E. H.; Cheianov, V. V.; Fal'ko, V. I.; Watanabe, K.; Taniguchi, T.; Gorbachev, R. V. *Nat. Phys.* **2011,** 7, 958-961.
7. Nomura, K.; MacDonald, A. *Phys. Rev. Lett.* **2006,** 96, 256602.
8. Young, A. F.; Dean, C. R.; Wang, L.; Ren, H.; Cadden-Zimansky, P.; Watanabe, K.; Taniguchi, T.; Hone, J.; Shepard, K. L.; Kim, P. *Nat. Phys.* **2012,** 8, 550-556.
9. Zhang, Y.; Jiang, Z.; Small, J.; Purewal, M.; Tan, Y.-W.; Fazlollahi, M.; Chudow, J.; Jaszczak, J.; Stormer, H.; Kim, P. *Phys. Rev. Lett.* **2006,** 96, 136806.
10. Elias, D. C.; Gorbachev, R. V.; Mayorov, A. S.; Morozov, S. V.; Zhukov, A. A.; Blake, P.; Ponomarenko, L. A.; Grigorieva, I. V.; Novoselov, K. S.; Guinea, F.; Geim, A. K. *Nat. Phys.* **2011,** 7, 701-704.
11. Chae, J.; Jung, S.; Young, A.; Dean, C.; Wang, L.; Gao, Y.; Watanabe, K.; Taniguchi, T.; Hone, J.; Shepard, K.; Kim, P.; Zhitenev, N.; Stroscio, J. *Phys. Rev. Lett.* **2012,** 109, 116802.
12. Hwang, C.; Siegel, D. A.; Mo, S.-K.; Regan, W.; Ismach, A.; Zhang, Y.; Zettl, A.; Lanzara, A. *Sci. Rep.* **2012,** 2, 590.
13. Yang, W.; Chen, G.; Shi, Z.; Liu, C.-C.; Zhang, L.; Xie, G.; Cheng, M.; Wang, D.; Yang, R.; Shi, D.; Watanabe, K.; Taniguchi, T.; Yao, Y.; Zhang, Y.; Zhang, G. *Nat. Mater.* **2013,** 12, 792-797.
14. Park, C. H.; Yang, L.; Son, Y. W.; Cohen, M. L.; Louie, S. G. *Nat. Phys.* **2008,** 4, 213-217.
15. Park, C.-H.; Yang, L.; Son, Y.-W.; Cohen, M. L.; Louie, S. G. *Phys. Rev. Lett.* **2008,** 101, 126804.
16. Yankowitz, M.; Xue, J. M.; Cormode, D.; Sanchez-Yamagishi, J. D.; Watanabe, K.; Taniguchi, T.; Jarillo-Herrero, P.; Jacquod, P.; LeRoy, B. J. *Nat. Phys.* **2012,** 8, 382-386.
17. Dean, C. R.; Wang, L.; Maher, P.; Forsythe, C.; Ghahari, F.; Gao, Y.; Katoch, J.; Ishigami, M.; Moon, P.; Koshino, M.; Taniguchi, T.; Watanabe, K.; Shepard, K. L.; Hone, J.; Kim, P. *Nature* **2013,** 497, 598-602.
18. Hunt, B.; Sanchez-Yamagishi, J. D.; Young, A. F.; Yankowitz, M.; LeRoy, B. J.; Watanabe, K.; Taniguchi, T.; Moon, P.; Koshino, M.; Jarillo-Herrero, P.; Ashoori, R. C. *Science* **2013,** 340, 1427-1430.
19. Ponomarenko, L. A.; Gorbachev, R. V.; Yu, G. L.; Elias, D. C.; Jalil, R.; Patel, A. A.; Mishchenko, A.; Mayorov, A. S.; Woods, C. R.; Wallbank, J. R.; Mucha-Kruczynski, M.; Piot, B. A.; Potemski, M.; Grigorieva, I. V.; Novoselov, K. S.; Guinea, F.; Fal'ko, V. I.; Geim, A. K. *Nature* **2013,** 497, 594-597.
20. Hofstadter, D. R. *Phys.Rev. B* **1976,** 14, 2239-2249.
21. Albrecht, C.; Smet, J. H.; von Klitzing, K.; Weiss, D.; Umansky, V.; Schweizer, H. *Physica E: Low-dimensional Systems and Nanostructures* **2003,** 20, 143-148.
22. Yu, G. L.; Gorbachev, R. V.; Tu, J. S.; Kretinin, A. V.; Cao, Y.; Jalil, R.; Withers, F.; Ponomarenko, L. A.; Piot, B. A.; Potemski, M.; Elias, D. C.; Chen, X.;

Watanabe, K.; Taniguchi, T.; Grigorieva, I. V.; Novoselov, K. S.; Fal/'ko, V. I.; Geim, A. K.; Mishchenko, A. *Nat. Phys.* **2014,** 10, 525-529.
23. Chen, X.; Wallbank, J. R.; Patel, A. A.; Mucha-Kruczyński, M.; McCann, E.; Fal'ko, V. I. *Physical Review B* **2014,** 89, 075401.
24. Wang, L.; Gao, Y.; Wen, B.; Han, Z.; Taniguchi, T.; Watanabe, K.; Koshino, M.; Hone, J.; Dean, C. R. *Science* **2015,** 350, 1231-1234.
25. Zhang, Y. B.; Tan, Y. W.; Stormer, H. L.; Kim, P. *Nature* **2005,** 438, 201-204.
26. Novoselov, K. S.; Geim, A. K.; Morozov, S. V.; Jiang, D.; Katsnelson, M. I.; Grigorieva, I. V.; Dubonos, S. V.; Firsov, A. A. *Nature* **2005,** 438, 197-200.
27. Bostwick, A.; Ohta, T.; Seyller, T.; Horn, K.; Rotenberg, E. *Nat. Phys.* **2007,** 3, 36-40.
28. Feldman, B. E.; Martin, J.; Yacoby, A. *Nat. Phys.* **2009,** 5, 889-893.
29. Wannier, G. H. *phys. status solidi b* **1978,** 88, 757-765.
30. Kotov, V. N.; Uchoa, B.; Pereira, V. M.; Guinea, F.; Castro Neto, A. H. *Rev. of Mod. Phys.* **2012,** 84, 1067-1125.
31. Berger, C.; Song, Z.; Li, X.; Wu, X.; Brown, N.; Naud, C.; Mayou, D.; Li, T.; Hass, J.; Marchenkov, A. N.; Conrad, E. H.; First, P. N.; de Heer, W. A. *Science* **2006,** 312, 1191-1196.
32. Young, A. F.; Kim, P. *Nat. Phys.* **2009,** 5, 222-226.
33. McCann, E.; Kechedzhi, K.; Fal'ko, V. I.; Suzuura, H.; Ando, T.; Altshuler, B. L. *Phys. Rev. Lett.* **2006,** 97, 146805.
34. Tikhonenko, F. V.; Horsell, D. W.; Gorbachev, R. V.; Savchenko, A. K. *Phys. Rev. Lett.* **2008,** 100, 056802.
35. Yan, X.-Z.; Ting, C. S. *Phys. Rev. Lett.* **2008,** 101, 126801.
36. Van Hove, L. *Phys. Rev.* **1953,** 89, 1189-1193.
37. Li, G.; Luican, A.; Lopes dos Santos, J. M. B.; Castro Neto, A. H.; Reina, A.; Kong, J.; Andrei, E. Y. *Nat. Phys.* **2010,** 6, 109-113.
38. Chen, Z.-G.; Shi, Z.; Yang, W.; Lu, X.; Lai, Y.; Yan, H.; Wang, F.; Zhang, G.; Li, Z. *Nat. Commun.* **2014,** 5, 4461.
39. Faugeras, C.; Berciaud, S.; Leszczynski, P.; Henni, Y.; Nogajewski, K.; Orlita, M.; Taniguchi, T.; Watanabe, K.; Forsythe, C.; Kim, P.; Jalil, R.; Geim, A. K.; Basko, D. M.; Potemski, M. *Phys. Rev. Lett.* **2015,** 114, 126804.

Figure legends

Figure 1| Graphene superlattice. a, Optical microscopy image of the device. **b**, AFM height image of graphene superlattice structure. **c**, Transfer curve at a temperature T =1.8 K, showing superlattice Dirac points at both electron and hole sides. The scale bars in **a**, **b** are 20 μm and 100 nm respectively.

Figure 2| Quantum Hall States in graphene superlattice. a, Landau fan diagram of R_{xx} as a function of back gate V_g and magnetic field B at T = 1.8K. The white dashed lines are guide eye for landau levels (LLs) with v = 2. **b**, Longitudinal (R_{xx}, Pink) and Hall resistance (R_{xy}, blue) versus gate voltage V_g at T = 1.8 K, B = 9 T, and the inset is the corresponding conductivity around Dirac point (DP).

Figure 3| Hofstadter butterfly spectra. a-b, Landau fan diagram of longitudinal conductivity σ_{xx} (**a**) and Hall conductivity σ_{xy} (**b**) as a function of V_g and magnetic field B at T = 1.8K. **c** shows zoomed in images of **a** (left) and **b** (right), with the dashes lines indicating LLs from DP (grey) and SDP (white) respectively. **d**, Observed Hofstadter butterfly spectra in Wannier diagram. The assignment of colors is as followed: black and blue lines indicate single-particle and many-body gaps (due to QHFM) from main DP respectively; green (no broken symmetry) and pink (broken symmetry) lines indicate Hofstadter gaps in the regime of strong superlattice influence; red lines indicate fractal gaps originated from replica Dirac spectra that are quantized in effective magnetic field $B_{eff} = \pm | B\text{-}B_{1/q} |$, and here q = 3, 4.

Figure 4| Metal insulator transition. a, Colored mapping of *R(T)/R(T=1.8K)* as a function of V_g (-60 to 60 V) and T (1.65 K-80 K). **b**, R_{xx} versus Vg for different T, and the inset is the temperature dependence of resistance at DP and SDPs . **c-e** are plots of *R(T)/R(T=1.8K)* over a wide range of carrier density, revealing a transition of metal to insulating behaviors away from charge neutral points (DP and SDPs).

Figure 5| Renormalization of Fermi velocity. a, Shubnikov–de Haas oscillations (SdHOs) with R_{xx} versus magnetic field B (0 to 9T) at V_g = -20 V for different T, and the inset displays the T-dependent SdH amplitude at B = 3T. **b**, Plot of Fermi velocity (v_F) as a function of B for different carrier density.

Figures

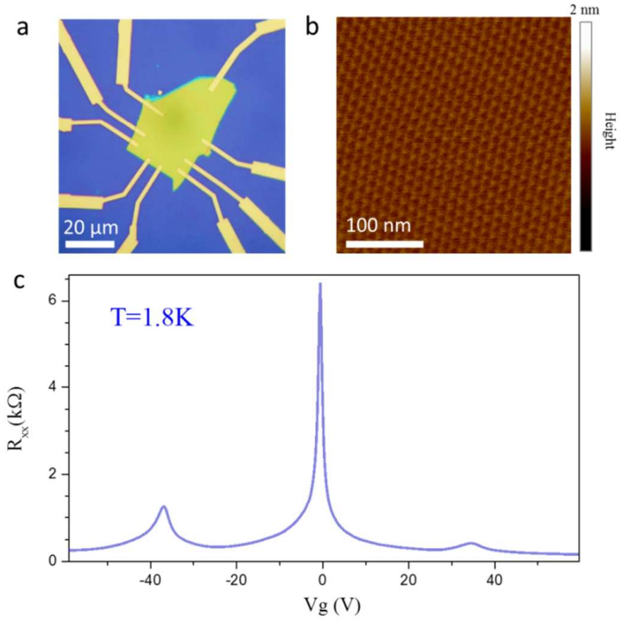

Figure 1 by W. Yang, *et al.*

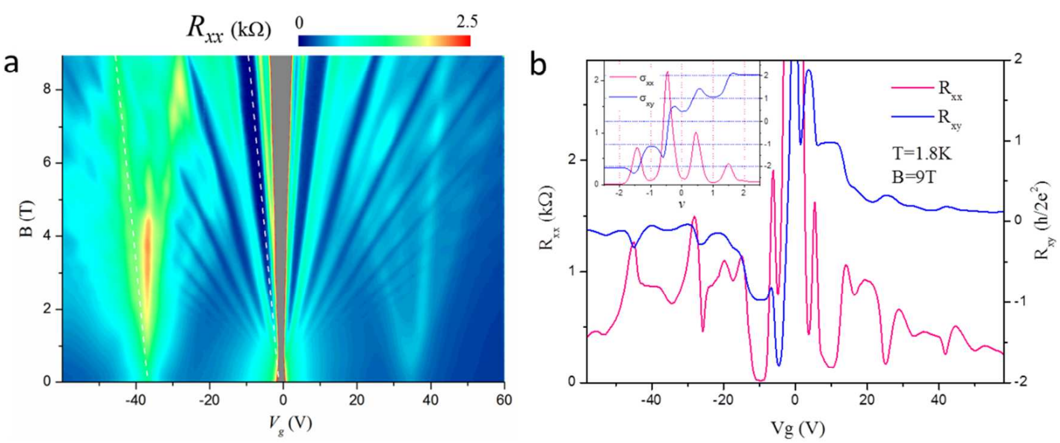

Figure 2 by W. Yang, *et al.*

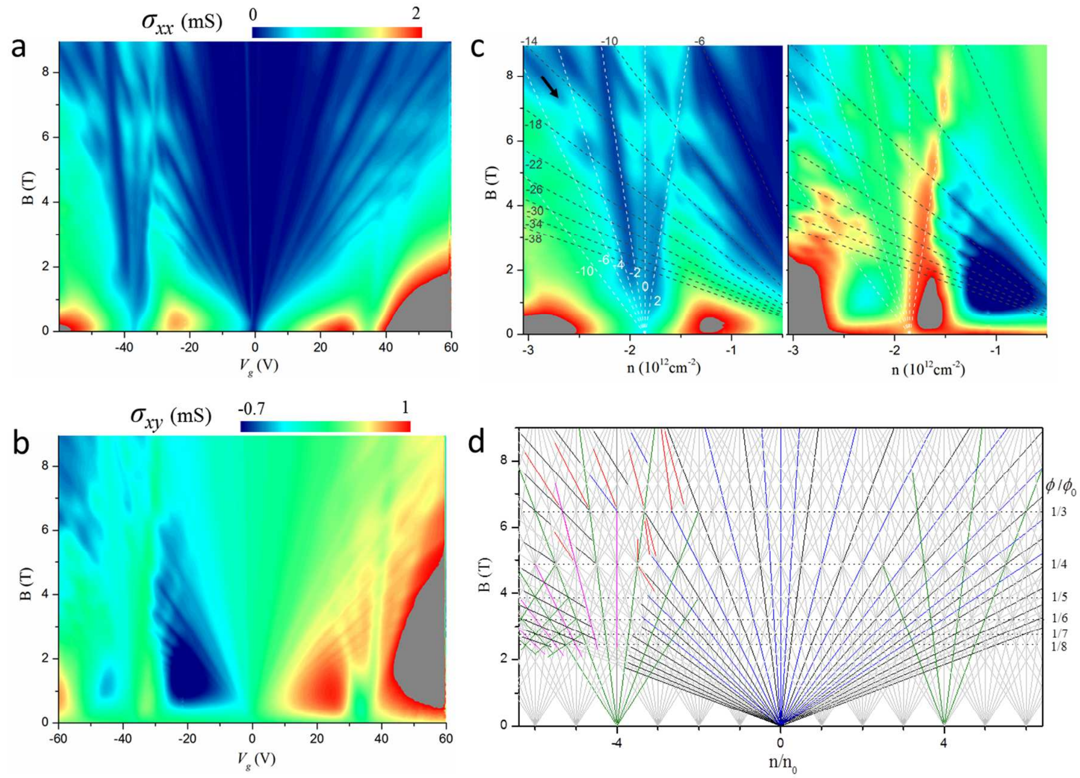

Figure 3 by W. Yang, *et al.*

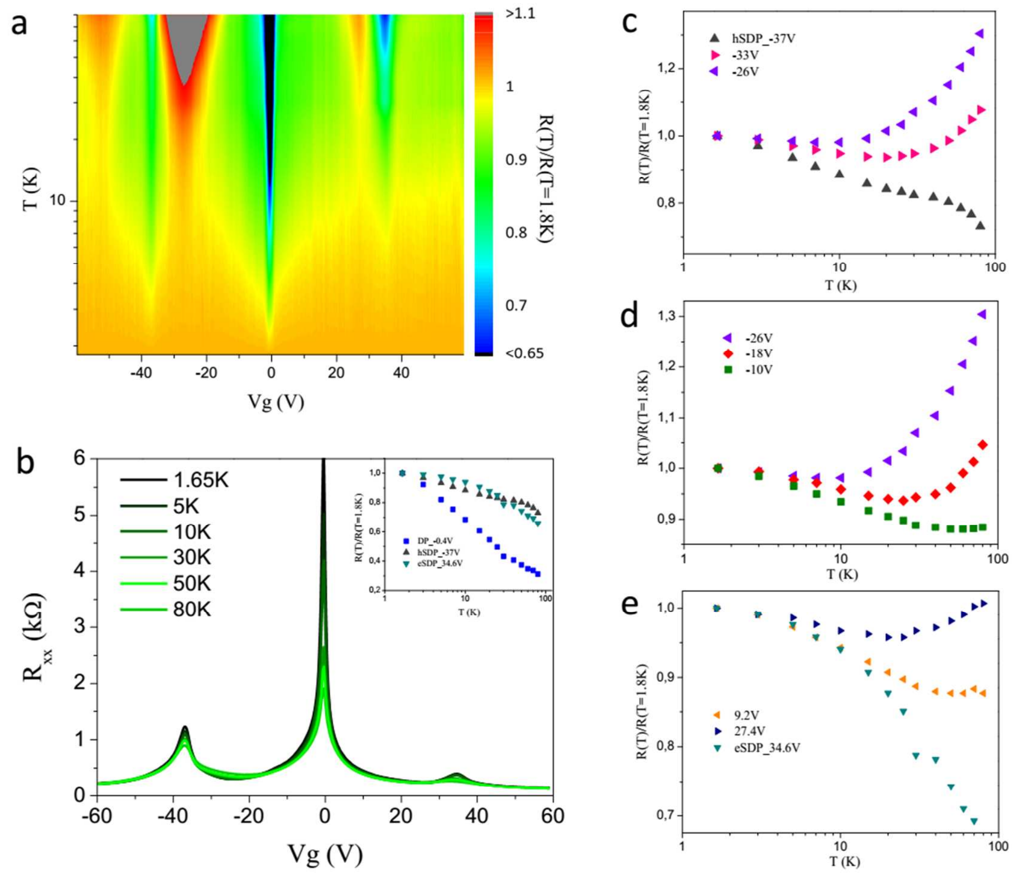

Figure 4 by W. Yang, *et al.*

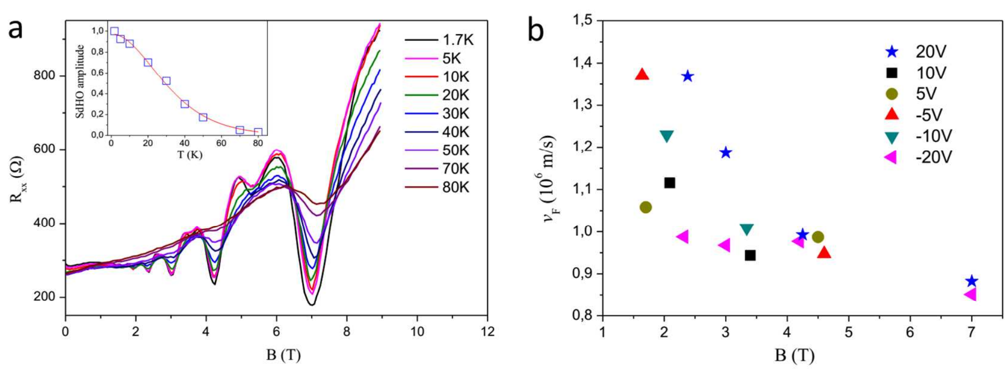

Figure 5 by W. Yang, *et al.*

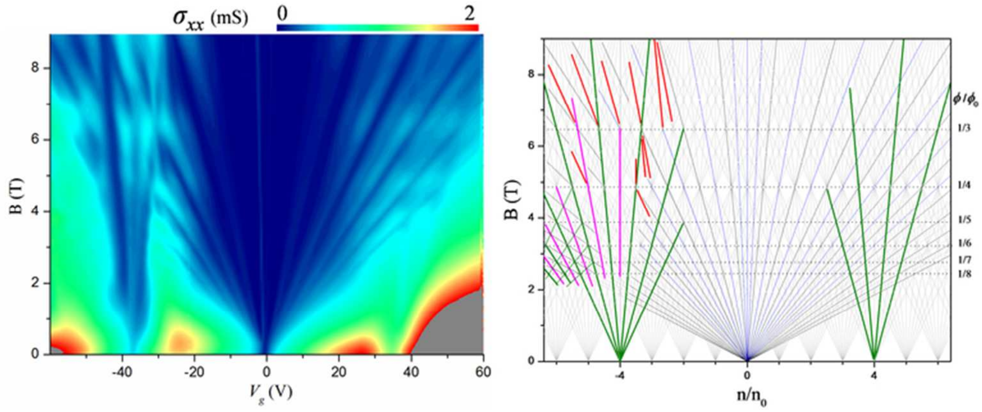

Table of Contents graphic
33x13mm (600 x 600 DPI)